ANALYTICAL MODEL FOR CONCRETE STRUCTURES INFLUENCED BY CRACK INITIATION AND PROPAGATION

(Translation from Proceedings of JSCE, No.620/V-43, May 1999)

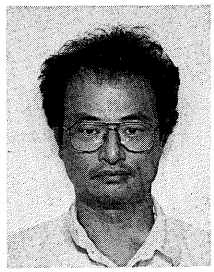
Shigeru MATSUOKA

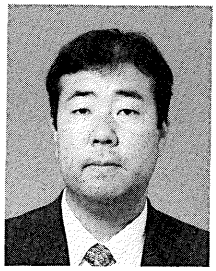
Akihisa MASUDA

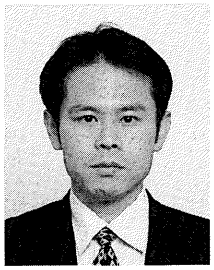
Yasushi TAKEDA

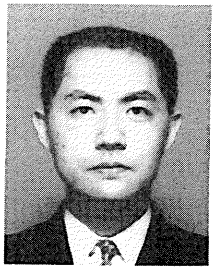
Shiro DOI

This paper proposes an analytical model for determining the fracture load of concrete structures whose deformation and fracture behaviors are governed by the occurrence and growth of cracks. The proposed model computes the evolution of cracks by considering the localization of cracking in brittle materials such as concrete. Furthermore, by modeling the relationship between stress transmitted to the crack interface and crack opening, it is possible to follow crack evolution under composite stresses. An analytical study of previous reinforced concrete experiments using the proposed model has demonstrated that the model is capable of determining the shear strength of reinforced concrete beams which undergo diagonal tensile fracture.

Key Words: *fracture mechanics, localization, smeared crack model, tension softening relationship*

Shigeru Matsuoka is an engineer in the Institute of Technology at TEKKEN Corporation. He obtained his D.Eng. from Tokyo University in 1999. His research interests relate to the fracturing of concrete structures. He is a member of the JSCE.

Akihisa Masuda is an engineer in the Institute of Technology at TEKKEN Corporation. His research interests relate to the fracturing of concrete structures. He is a member of the JSCE.

Yasushi Takeda is an engineer in the Institute of Technology at TEKKEN Corporation. His research interests relate to the fracturing of concrete structures. He is a member of the JSCE.

Shiro Doi is an engineer in the Institute of Technology at TEKKEN Corporation. He obtained his MS from Kyushu University in 1995. His research interests relate to the fracturing of concrete structures. He is a member of the JSCE.

---

1. INTRODUCTION

It is reported that, since concrete fracturing is dominated by cracks and their propagation, a fracture mechanics that describes the mechanical behavior related to crack initiation and propagation would be effective for the structural analysis of concrete [1]. Aiming at an application of fracture mechanics to concrete, cracking has been investigated for its mechanical properties. As for what is called a Mode I fracture, where the tensile stress acts normally to the crack faces, some papers have reported that, by considering a tension softening curve that represents the relationship between crack width and tensile strength, it is possible to follow the occurrence and progression of cracking.

Uchida et al. [2] demonstrated that the size effect of concrete bending tensile strength can be computed by resorting to tension softening curves. On the other hand, Japan Railway Construction Public Corporation publishes guidelines for the design and construction of tunnel linings [3] based on fracture mechanics. As this demonstrates, concrete fracture mechanics has entered the realm of practical application founded an basic investigations.

Niwa et al. [4] studied the size effect on the shear strength of reinforced concrete beams using a discrete crack model that considers the softening of tensile stress in cracked surfaces. An et al. [5] analyzed the size effect on the shear strength using a distributed crack model. In this analytical model, two different zones are assumed in a reinforced concrete beam : an RC zone and a PL zone. In the RC zone, transmission of tensile stress is expected to continue even after cracking due to bonding with reinforcement. In the PL zone, the tensile stress abruptly softens on crack initiation. This model, unlike the analytical technique proposed by Niwa et al., considers not solely tension softening, but also shear softening, in terms of stress transmission at the crack interface. The report by An et al. demonstrates that it is possible, by using an analytical model involving the transmission of tensile and shear stresses in the crack faces, to compute the size effect of shear strength of RC beams.

However, for a discrete crack model, setting up crack propagation trajectories is an essential problem, since the behavior of concrete after reaching the maximum crack producing load varies with the crack propagation trajectories. On the other hand, the smeared crack model assumes that cracking occurs when the stress reaches a certain level. Accordingly, by computation, it appears that numerous cracks may occur. In actual concrete, however, a phenomenon called "crack localization" takes place; that is, the number of cracks which actually propagate is limited. It is therefore vital to evaluate crack localization when conducting analysis by a smeared crack model.

The present study discusses a smeared crack model that includes crack localization. An analytical model is investigated that is applicable to mixed mode fractures where Mode II fractures and Mode I fractures occur simultaneously. Mode II refers to the state where the shear force at crack faces acts normally to the crack tip line. By using this model, computations on RC beams are conducted to demonstrate that this analytical technique is capable of assessing the size dependency of shear strength.

2. ANALYTICAL TECHNIQUES FOR CRACK INITIATION AND PROPAGATION

2.1 Tensile Fracture Characteristics of Concrete

It can be assumed that a fracture process zone exists at the crack tip, as shown in Fig.1. The fracture process zone is divided into a microcracking zone governed by progressive microcracks and a bridging zone governed by bridging between aggregates. In both zones, stress transmission is assumed to take place. The stress transmitted in the fracture process zone depends upon the crack opening width, as illustrated in Fig. 1. The relationship between stress and crack opening is called the tension softening curve. Hordijk [6] proposed, on the basis of tensile test results for concrete, an approximation of the tension softening curve as Eq.(1).

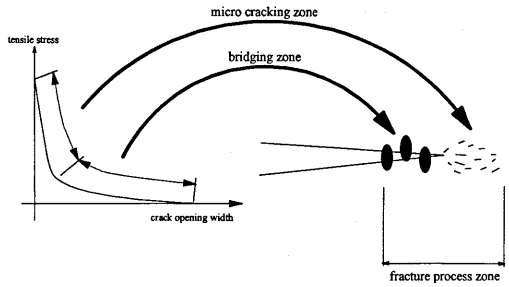

Fig.1 Fracture Process Zone

$$\frac{\sigma_t}{f_t} = \left\{1 + \left[C_1 \frac{w}{w_c}\right]^3\right\} \exp\left[-C_2 \frac{w}{w_c}\right] - \frac{w}{w_c}\left[1 + C_1^3\right]\exp(-C_2) \quad (1)$$

where C_1=3, C_2=6.93, w represents the crack opening, w_c is the limit opening (=160μm), f_t is the tensile strength of concrete, σ_t is the tensile stress at crack opening w. Horii [7] showed that the gradient of the tension softening curve immediately after crack initiation is a key parameter, and reported that the maximum concrete load can be conservatively approximated to a satisfactory accuracy by a model consisting of a linear equation with a gradient equal to the tangent of the tension softening curve just after crack initiation. Further, Planas et al. [8] addressed, on the basis of experiments and analysis, an effective approximation of the maximum concrete load using a model consisting of a straight line whose gradient is that of the tension softening curve immediately after crack initiation. In order to study the effect of the tension softening curve, we conducted a computation as illustrated in Fig. 2 with a 4-point bending test model. Three tension softening curves were involved in this analysis, as shown in Fig. 3; the equation given by Hordjik (Eq.1), a linear model with the gradient just after crack initiation, and a bilinear model. The graphs in Fig. 4 are the relationships between bending strength and sectional depth. The computation results are as follows. Hordjik's equation, by which the fracture energy (represented by the area under the curve) is the largest, provides the greatest bending strength. However, the difference in bending strength with type of tension softening curve tends to decrease with increasing depth. As for the same size effect on the bending test, almost the same tendency is observed for the three tension softening curves. As these results demonstrate, when the linear model representing a smaller fracture energy is used, the maximum load is smaller than the results with other models, whereas the size effect is almost the same with all the models. Since we aim at studying the behavior of concrete structures as cracks occurr and grow, the tensile failure characteristic is expressed by the linear model with the gradient corresponding to the tangent to Eq.(1) at a point just after crack initiation, as proposed by Hordjik and shown in Fig.3.

Our analysis assumes that, when the major principal stress (tension is expressed as positive) reaches the tensile strength of the concrete, crack occurs normally to the major principal stress direction. Modeling was done supposing that the deformation normal to the crack face in cracked elements is the sum of crack opening and elastic deformation other than cracking. It was therefore assumed that the tensile stress-strain relationship normal to the crack face can be expressed by the tension softening curve, which expresses the tensile fracture characteristics of the crack face, and the stress-strain

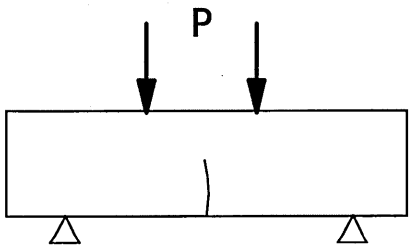

Fig.2 4-point Bending Test

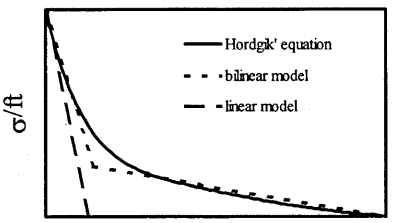

Fig.3 Model of Tension Softening Curve

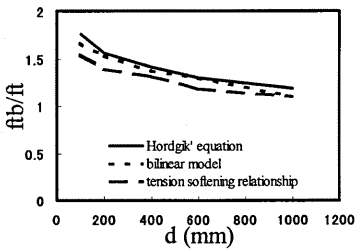

Fig.4 Relationships between Bending Strength and Sectional Depth

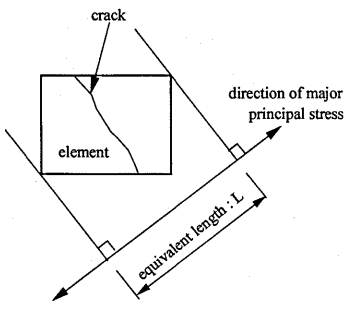

Fig.5 Equivalent Length

relationship in the elastic zone outside the cracked zone. To eliminate dependence on element size in converting the tension softening curve to a stress-strain relationship, the concept of "equivalent length" is introduced; this is the length of the element projected normally on to the major principal stress direction, as shown in Fig.5. The strain normal to the crack face in the cracked elements is given by Eq.(2).

$$\varepsilon_{ct} = \frac{\sigma_t}{E_t} + \frac{w(\sigma_t)}{L} \tag{2}$$

where ε_{ct} is the strain in the major principal stress direction in the cracked elements, σt is the major principal stress in the cracked elements, E_t is the elastic modulus of the concrete on the tension side, $w(\sigma_t)$ is the crack opening determined by the major principal stress σ_t from the tension softening curve, and L is the equivalent length of the cracked element.

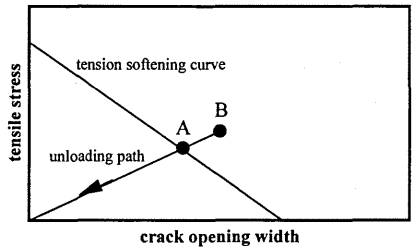

Fig.6 Judgment of Crack Localization

In studying crack localization in brittle materials such as concrete, it is necessary to judge whether the tensile characteristics of cracked elements fall on the unloading path or on the tension softening curve. In the present study, if a cracked element is at point A on the tension softening curve in Fig.6, then at the next step, the calculation is conducted supposing that the element is on the unloading path directed toward the origin. In this incremental computation, when the tensile characteristic of the cracked element falls at a point off the tension softening curve, such as point B in Fig.6, the computation is done again by treating its tensile characteristic as being on the tension softening curve instead of on the unloading path. By such repetitive computations, crack localization is evaluated. The authors [9] have already demonstrated, by referring to experimental results, that such repetitive computations are an effective means of expressing localized cracks in concrete members.

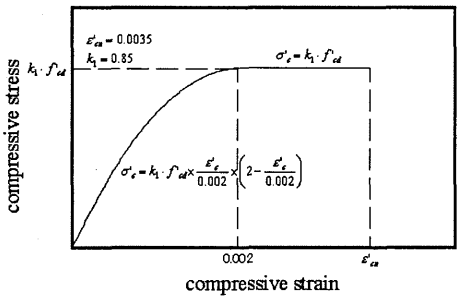

Fig.7 Compressive Stress-Strain Relationship

A compressive stress-strain curve of quadratic type was selected, as shown in Fig.7. A Drucker-Prager yield surface was used. By treating the compressive stress-strain relationship as uni-axial test results, the constant of the yield surface is determined.

2.2 Shear Stiffness of Cracked Elements

In the mixed fracture mode (Mode I plus Mode II), shear stress parallel to the crack faces and tensile stress normal to the crack faces are both in effect. It is assumed that, in this state, displacement occurs parallel and normal to the crack faces, as shown in Fig.8, and the crack opening can be expressed by Eq.3.

$$\delta_{cr} = \sqrt{\delta_x^2 + \delta_y^2} \tag{3}$$

where δ_{cr} is the crack opening, δ_x is the cracking displacement in the X direction, and δ_y is the cracking displacement in the Y direction. Using this crack opening width, analysis was carried out assuming that elements other than the cracked elements are rigid, as shown in Fig.8. In this analytical procedure, first the displacement δ_y is given in the X direction, which is normal to the crack face, then by keeping δ_x constant, displacement δ_y was increased in the Y direction parallel to the crack face.

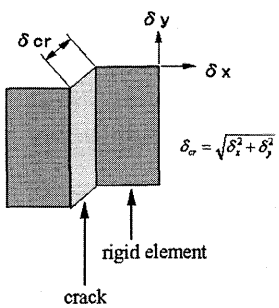

Fig.8 Concept of Crack Opening

Since, according to Eq(3), the crack opening increases with displacement in the Y direction, the nodal force P_x in the X direction decreases with increasing the Y direction displacement, as shown in Fig.9. In contrast, the nodal force P_y in the Y direction increases with displacement, then decreases as shown in Fig.9.

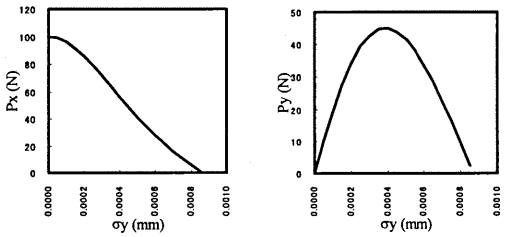

Fig.9 Relationships between Displacement and Force in the Crack Face Using Discrete Crack Model

Since, in the smeared crack model, the cracked elements too are assumed to be a continuum, the body force per unit area of infinitesimal element is given by Eq.(4).

$$F_x + \frac{\partial \sigma_x}{\partial x} + \frac{\partial \tau_{xy}}{\partial y} = 0$$
$$F_y + \frac{\partial \sigma_y}{\partial y} + \frac{\partial \tau_{xy}}{\partial x} = 0 \qquad (4)$$

where F_x is the body force in the X direction and F_y is the body force in the Y direction. The stress of each component is obtained from the displacement components by Eqs.(5) and (6).

$$\begin{bmatrix} \sigma_x \\ \sigma_y \\ \tau_{xy} \end{bmatrix} = D \cdot \begin{bmatrix} \varepsilon_x \\ \varepsilon_y \\ \gamma_{xy} \end{bmatrix} \qquad (5)$$

$$\begin{bmatrix} \varepsilon_x \\ \varepsilon_y \\ \gamma_{xy} \end{bmatrix} = \begin{bmatrix} \frac{\partial}{\partial x} & 0 \\ 0 & \frac{\partial}{\partial y} \\ \frac{\partial}{\partial y} & \frac{\partial}{\partial x} \end{bmatrix} \cdot \begin{bmatrix} \delta_x \\ \delta_y \end{bmatrix} \qquad (6)$$

Holding δ_x constant, there is no increase in δ_x as is clear from Eq.(6). With constant δ_x and increasing δ_y, F_x mainly depends on the shear stress alone. To achieve a decrease in P_x as shown in Fig.9 by the smeared crack model, it is necessary to vary the shear stress. If the cracked elements have no shear stiffness, the shear stress does not vary. Hence, in such a case, P_x is kept constant independently of δ_y.

From the discussion above, we can assume that the shear stiffness of cracked elements depends upon the crack opening in the smeared crack model; the crack opening being the displacement in the major principal stress direction minus the elastic deformation. Here, the shear retention factor is introduced, as determined using Eq.(7). This is a dimensionless expression of the shear stiffness of the cracked elements in terms of the shear stiffness before cracking.

$$\beta = \exp(-\alpha \cdot w) \qquad (7)$$

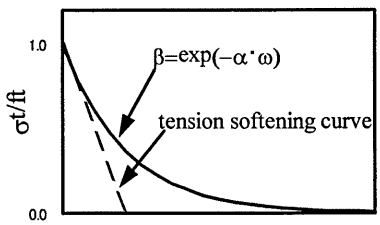

Fig.10 Definition of Shear Retention Factor

where β is the shear retention factor, α is the decrease rate of shear retention factor, and w is the crack opening width. The crack opening is the displacement of an element in the major principal stress direction. The decrease rate of shear retention factor is determined such that the gradient of the shear retention factor just after crack initiation is equal to the gradient of the tension softening curve, as shown in Fig.10.

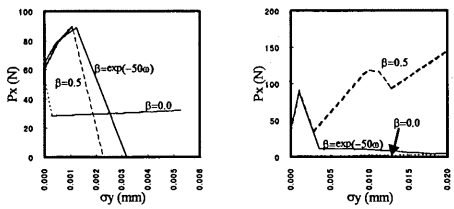

Fig.11 Relationships between Displacement and Force in Crack Face Using Smeared Crack Model

Supposing the shear stiffness of the cracked elements can be expressed by Eq.(7), the relationship between

displacement of cracked elements and force is computed as in the case of the discrete crack model in Fig.9. The computation results are summarized in Fig.11. Px decreases with increasing δ_y when Eq.(7) is applied and when the shear retention factor is constant. This result approximately agrees with the analytical results obtained with the discrete crack model. In contrast, in the case with no shear stiffness in the cracked elements, that is, with zero shear retention factor, P_x decreases abruptly on crack initiation, then remains almost constant. This behavior is different from the results of numerical analysis by the discrete crack model.

Now let us take a look at P_y. With a constant shear retention factor, the shear deformation becomes greater with increasing δ_y, and the nodal force P_y increases after a certain amount of displacement is reached. This is different from the result obtained by discrete crack model analysis. In contrast, with the shear retention factor given by Eq.(7), P_y too decreases with increasing displacement, as with the discrete crack model.

Thus, the model in which the shear stiffness of the cracked elements is given by Eq.(7) offers results similar to those obtained whit the discrete crack model.

3. VERIFICATION OF ANALYTICAL TECHNIQUES

3.1 Rumanian Shear Test

The authors [9] have confirmed the applicability of the proposed analytical model to the problem of fractures determined by Mode I. In this section, we discuss its applicability to mixed Mode I plus Mode II fractures.

The Rumanian shear test is an example of crack initiation and growth in a state other than pure tension. This test, as sketched in Fig.12, uses a test specimen notched at the center; loading is conducted in such a manner that the loading point does not coincide with the support point in the horizontal plane. Arrea et al. [10] reported that curvilinear cracks occur from the notch tip toward the loading point. We analyzed this test using the proposed model, inputting the physical properties given in Table 1. As regards compressive strength, no mention of this was found in the report. Thus, it was obtained from the tensile strength by Eq.(8) proposed by Koenig [11].

$$f_t = 2.12 \times \ln(1+\frac{f_c}{10}) \qquad (8)$$

where f_t is the tensile strength (N/mm^2) and f_c is the compressive strength (N/mm^2).

Analysis was conducted for a case with a falling shear retention factor following Eq.(7), and for a case with a constant retention factor. Figure 13 is a comparison of the analytical and experimental values as expressed by the relationship between amount of sliding at the notch and load magnitude.

As for the analytical results with falling shear retention factor, the maximum load obtained shows good agreement with the experimental values. The post-peak behavior, whereby the load decreases with increasing CMSD (Crack Mouth Sliding Displacement), is also similar to the experimental results. However, when the CMSD reaches 0.068 mm, the analysis ends since the crack penetrates, as illustrated in white in Fig.14. It is impossible to continue computations when the crack opening reaches a certain amount, resulting in almost no

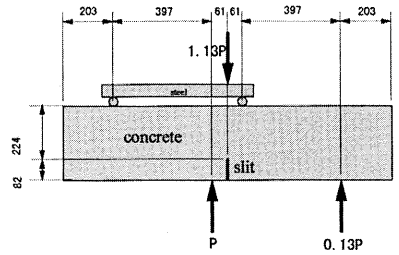

Fig.12 Schematic Diagram of Shear Test

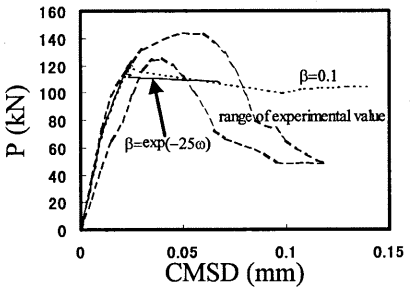

Fig.13 Relationships between Load and Displacement

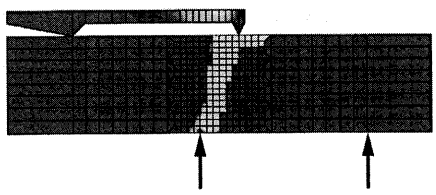
Fig.14 Cracking State

stress transmission. This end point can be considered rational, since it is located with the range of the experimental value distribution.

In the analytical case with constant shear retention factor, the maximum load is near the experimental value, and it is also near the numerical result with falling shear retention factor, but the CMSD continues increasing, even after the peak load, till a relatively large displacement occurs. This is because it is possible to continue computation since shear stress transmission takes place in the crack faces even after the crack penetrates the specimen. Figure 15 shows the numerical results beyond the stage given in Fig.13, with β=0.3 and 0.5 in addition to β=0.1. In every case, complex behavior is observed, with increasing and decreasing load and displacement. Such behavior does not reflect to the experimental behavior. Further, computations seemed to continue endlessly in every case, so the end point was obtained by a forced finish. The maximum load is not noticeably influenced by the shear retention factor, as is known from Table 2.

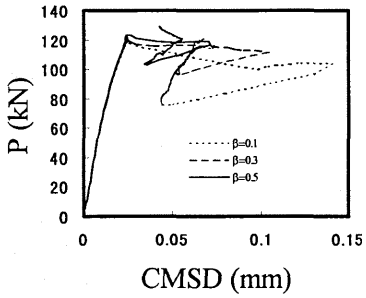

Fig.15 Relationships between Load and Displacement (β Is Fixed)

Table 2 Maximum Load in Case of Constant β

β	maximum load (kN)
0.1	119.484
0.3	119.867
0.5	120.367

As discussed above, with a constant shear retention factor, computation continues in a stable manner even when the displacement increases. However, the results of such computation may not agree well with the actual phenomenon. In contrast, the analytical results with falling shear retention factor proposed here approximately agree with the experimental maximum load, and the computation ends when the crack penetrates.

3.2 Anchor Bolt Pull-Out Test

Helbing et al. [12] conducted a test using the test specimen illustrated in Fig.16. For this test, an anchor bolt is embedded in a flat concrete panel, and then pulled out. The parameter of this test is the distance between the anchor bolt and the support point. The authors report a difference in crack initiation and propagation trajectory in relation to this parameter.

Table 3 summarizes the test specimen dimensions and material properties used for the pull-out test. It is reported that, cracks propagate from the anchor bolt end toward the support point. This test was analyzed by the model proposed in the present paper.

Helibing et al. report only one tensile fracture characteristic of concrete; that is, fracture energy G_F. Thus, the tension softening curve used for the analysis was determined as follows.

First, the tensile strength was obtained from the fracture energy, supposing that the tension softening curve of concrete follows the equation proposed by Hordijk, as shown in Fig.17. This tensile strength value was applied to the bilinear model created by back analysis by Wittmann et al. [13]. Of the two lines, the line having the 1st gradient was selected as the tension softening curve for this analysis. Referring to the tension softening curve, the shear retention factor was assumed to be given by Eq.(9).

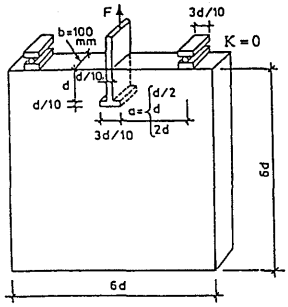

Fig.16 Schematic Diagram of Anchor Bolt Pull-Out Test

Table 3 Test Specimen Dimensions and Physical Properties

test variation	S1	S2	S3
d (mm)	150		
a (mm)	300	150	75
fc (N/mm^2)	39.3		
E (N/mm^2)	37600		
Gf (N/m)	93.17		

$$\beta = \exp(-33w) \qquad (9)$$

Three series of tests were conducted, taking as a parameter the distance between the anchor bolt and the support point. Figure 18 shows the load-displacement curves, both analytical and experimental. Table 4 summarizes the displacements at the maximum load and the magnitudes of the maximum loads, again both analytical and experimental. Since three tests were carried out under the same conditions in the pull-out test, the values in the table are the average and range of these test results.

As for the magnitude of the maximum load, the analytical value agrees relatively well with the experimental value for all three cases. Regarding the displacement at maximum load, too, the numerical results for patterns S2 and S3 are near the experimental results, while the analytical output for the S1 pattern is significantly different from the experimental value.

The white portions in Fig.19 show the cracking at maximum load and ultimate phase as given by the analysis of S2. At the maximum load, a curvilinear crack runs from the anchor end toward the support point, reaching approximately the center point between the anchor end and the support point. By continuing the analysis up to the ultimate phase, the crack coming from the anchor end reaches the support point, and consequently stress transmission across the crack faces falls to zero so the computation stops. In this phase, in addition to the above crack, a further crack propagates downward from the anchor end, and another runs diagonally downward, branching out from the crack between the anchor end and the support point.

The diagrams in Fig.20 represent the crack propagation observed in the analysis and experiments. The numerical results show a crack propagation trajectory from the anchor end toward the support point for all patterns; a crack branching from it and running diagonally downward for S1 and S2, and a crack

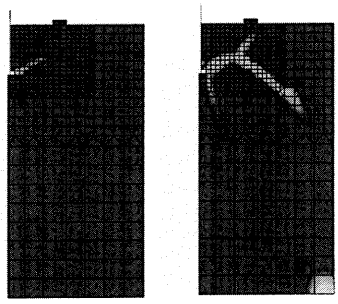

at maximum load at ultimate phase

Fig.19 Cracking Status (Analytical : S2)

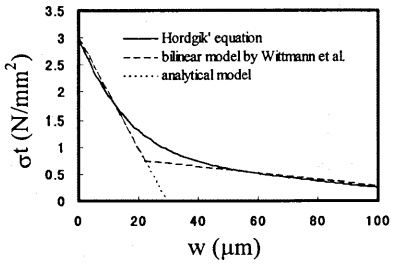

Fig.17 Tension Softening Curve for Analysis

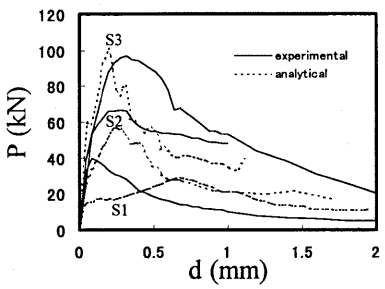

Fig.18 Relationships between Load and Displacement

Table 4 Displacement at Maximum Load

	experimental		analytical	
	load (kN)	displacement (mm)	load (kN)	displacement (mm)
S1:a=2d	38.4±1.8	0.083	29.0	0.694
S2:a=d	61.9±5.2	0.255	57.4	0.242
S3:a=d/2	117.1±12.6	0.248	100.8	0.197

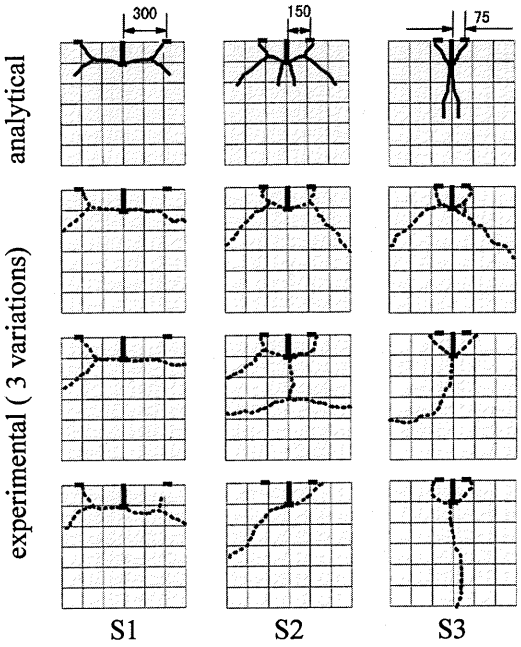

Fig.20 Cracking State

extending downward from the anchor end for S2 and S3. Since the analytical model is symmetrical, the cracking is symmetrical.

On the other hand, the experimental results show cracks in S2 and S3 that are almost symmetrical about the anchor bolt, aside from a few. This propagation is approximately equivalent to the analytical results. Contrarily, the cracking in the experimental result for S1 is not symmetrical. The crack on the side opposite the crack between the anchor end and support point tends to propagate from the anchor end toward the side of the concrete. This difference in cracking trajectory may be the cause for the different displacement numerically determined at the maximum load of S1. The paper [12] mentioned above does not discuss the cause of the asymmetric cracking trajectory observed in the experiment.

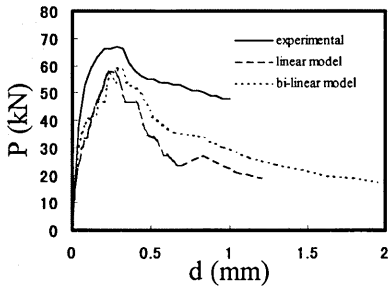

Fig.21 Influence of Relationships between Load and Displacement with Various Tension Softening Curves

To determine the influence of different tension softening curves, we computed values for S2 using the bilinear model shown in Fig.17. This computation yielded the result, shown in Fig.21, that the maximum load is almost the same as that by the linear model. However, the rate of load decrease is different after the maximum load is reached; that is, the computation with the bilinear model provides a curve with a more gentle decrease rate, agreeing somewhat better with the experimental load-displacement curve. This result suggests the possibility that the larger post-peak load decrease given by the linear model is attributable to the modeling of the tension softening curve.

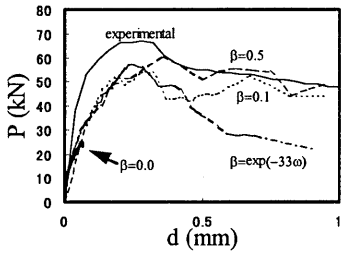

Fig.22 Relationships between Load and Displacement (S2)

For a comparative study on the influence of shear retention factor, analysis was conducted with a constant retention factor (β=0, 0.1, 0.5). As known from Fig. 22, with β=0, the maximum load is smaller than that with decreasing retention factor, so that the computation ends at a remarkably early stage. With β=0.1, the maximum load is almost equal to that with decreasing retention factor, but the post-peak load decrease is smaller than in the case of decreasing shear retention factor. Looking at the case in Fig.23, with β=0, cracking is observed only at the anchor bolt end, but at the ultimate stage the crack suddenly runs toward the support point. With β=0.1, crack initiation and propagation are almost the same as the numerical results for decreasing shear stiffness retention factor, and the computation continues stably even after the crack coming from the anchor bolt reaches the support point. Consequently, as shown in Fig.23, the cracked zone increases after the crack finally reaches the support point. With the constant retention factor, even when the crack opening becomes great, the shear stress is transmitted across cracked elements; therefore, it is possible to continue computation even after the crack attains the support point, resulting in the enlarged cracked area.

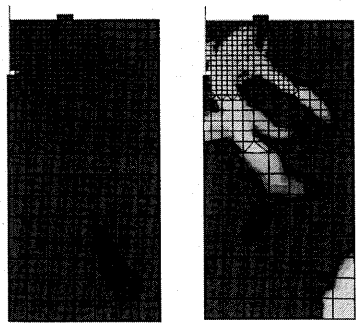

β=0 β=0.1

Fig.23 Cracking Status at Ultimate Phase (S2 : β is fixed)

As discussed above, by decreasing the shear retention factor in the cracked elements as proposed here, it is possible to approximate the anchor-bolt pull-out test.

3.3 Bonding between Reinforcement and Concrete

The discussion in the previous sections solely concerns plain concrete. To make the proposed model applicable also to RC structures, it is necessary to study the bonding between concrete and reinforcing bars. Accordingly, we conducted analysis of the tensile tests carried out by Shima et al. [14] on the reinforcement embedded in concrete, to verify the applicability of the model.

Figure 24 is a schematic diagram of the test specimen. Table 5 gives the properties of the test specimen materials. The analysis covered two types of test which differed from each other in reinforcement material alone. The reinforcing bars are considered to be truss elements that do not withstand bending. Since the analysis is aimed at mapping RC beam shear fractures due to diagonal cracking, a perfect elasto-plastic model is created to represent the reinforcement. The tensile strength was estimated from the compressive strength using Eq.(8). For the tension softening curve, a linear model is used, with a gradient equal to the tangent in Eq.(1) as proposed by Hordijk [6]. The shear retention factor given by Eq.(10) is applied, as obtained from the tension softening curve.

$$\beta = \exp(-50w) \tag{10}$$

The graphs in Fig.25 are load-displacement curves constructed from both the experimental and numerical results. The loads are reinforcement tensions. The displacements are average strains obtained by dividing the reinforcing bar displacement by the specimen length. The experimental results show that, in the range of average strain up to around 0.1%, the concrete undergoes fracture, resulting in reduced bonding with the reinforcement. When the strain exceeds 0.2%, no bonding remains, and the load is borne by the reinforcement alone. It can be considered, therefore, that the maximum load depends on the nature of the reinforcing bar material. When the reinforcing bars yield, the load increase becomes extremely gentle.

The numerical results are summarized as follows. There is a region for both cases in which the load fluctuates somewhat around 0.1 MN, while the average strain alone increases. This region corresponds to the phase in which cracks normal to the reinforcement appear successively from both ends of the specimen and propagate toward the center at certain intervals. Ultimately, cracks are distributed with almost uniform spacing over the whole of the specimen, and the load stops fluctuating, as shown in white in Fig.26. It can be said that this region depends on the characteristics of the concrete. The observed fluctuations agree well with the experimental results. After this phase, the load increases due to the rigidity of the reinforcing bars, and ultimately the bars yield, and there is no load

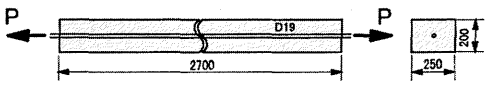

Fig.24 Schematic Diagram of Tensile Test of Reinforcement Embedded in Concrete

Table 5 Test Specimen Physical Properties

Pattern	Compressive stress of concrete (N/mm^2)	ratio of tension bar (%)	yield strebth of bar (N/mm^2)	elastic modulus of bar (N/mm^2)
A	25	0.6	610	190000
B			350	

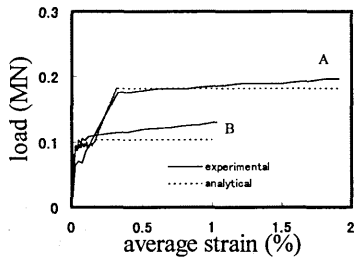

Fig.25 Relationships between Load and Strain

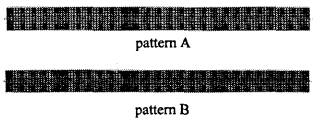

Fig.26 Cracking State (Analytical)

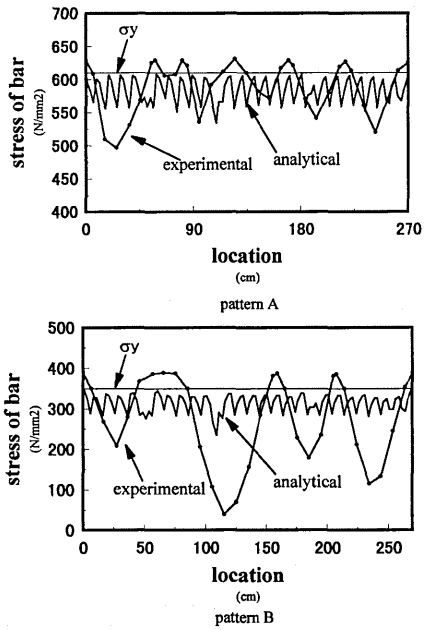

Fig.27 Distribution of Stress in Bar

increase at all. This latter behavior is obtained because the analysis assumes the stress-strain relationship of reinforcing bars is perfectly elasto-plastic. However, it can be concluded that there is good agreement between analytical and experimental results.

Figure 27 is the distribution of stress in the reinforcement immediately after yielding. The experimental results show, for both patterns, an undulating distribution of stresses around the yield stress. That is to say, the stress reaches the yield point at multiple locations, leading to broken bonding between reinforcement and concrete, and consequently resulting in the whole length of the bar reaching the near-yield state. The analytical stress distributions have smaller undulating cycles, which reach to nearly one half of the specimen sectional depth. Almost all stress magnitudes are below the yield point. But, some reach the yield point, and this may be why there is no increase in load. Such a state corresponds to cracking of the concrete as shown in Fig. 26, where the cracks occur at some interval due to bending of the RC beams. This is because, in elements in contact with the reinforcement, cracks are produced as the reinforcement elongates, forming lower bonding regions around the reinforcement.

As discussed above, the lower bonding regions are localized around the reinforcement, so the model proposed here is capable of evaluating the apparent sliding displacement between reinforcement and concrete.

4. APPLICATION TO ENGINEERING PROBLEMS

In the previous sections, the applicability of the proposed analytical model was studied in reference to the mixed fracture mode and reinforcement bonding, respectively. This section discusses the applicability of the same model to more realistic structures where such conditions exist in composite arrangements.

4.1 Size Effect of Shear Strength

Iguro et al. [15] reported on the size effect of shear strength, on the basis of bending tests with RC beam specimens of 10 cm to 300 cm in effective sectional depth and not provided with shear reinforcement. Figure 28 shows schematically the bending test and Table 6 lists the specifications and properties, such as the sectional dimensions. The proposed analytical model was applied to these experiments. Since the concrete strength slightly varies from one specimen to another, as seen in Table 6, the analysis was based on the figure of 23.5 MPa, which is the required average strength. The shear retention factor given by Eq.(10) was used. Since the purpose of this analysis is to understand the size effect on the shear strength of reinforced concrete, a linear model with a gradient of 128N/mm^3 was used as the tension softening curve.

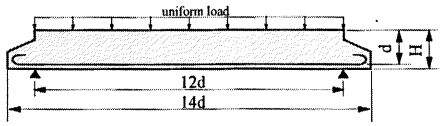

Fig.28 Schematic Diagram of Bending Test

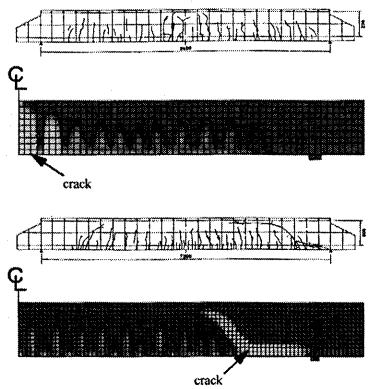

Fig.29 Cracking Status (Experimental and Analytical)

Table 6 Test Specimen Dimensions and Physical Properties

test specimen dimensions						concrete			reinforcement		
effective height d(cm)	load span 12d(cm)	ratio of load span	length 14d(cm)	heigh H(cm)	width b(cm)	maximum size of coarse aggregate (mm)	compressive strength (N/mm^2)	tensile strength (N/mm^2)	diameter & numbers	ratio of axial bar	yield strength (N/mm^2)
10	120		140	12	15.8		20.6	1.85	D6×2		
20	240		280	22	15.8	10	19.7	1.87	D6×4		440
60	720		840	65.5	30		21.1	1.81	D6×24		
100	1200	12	1400	120	50		27.2	2.05	D10×28	0.4	
100	1200		1400	120	50		21.9	2.23	D10×28		370
200	2400		2800	210	100	25	28.5	2.73	D16×40		
300	3600		4200	314	150		24.3	2.19	D25×36		360

According to Iguro et al., with specimens of 20cm or less in effective sectional depth, the axial reinforcement yields, so the strength is determined by the bending fracture. On the other hand, with specimens of 60 cm or more in sectional depth, shear fracturing was observed, where the strength is determined by diagonal crack initiation and propagation. For example, no diagonal cracking is seen in the specimen with an effective sectional depth of 20cm shown in Fig.29. In contrast, diagonal cracking is observed in the 60cm specimen. Such a cracking pattern suggests that a shear fracture takes place.

The diagrams in Fig.29 depict the cracking status numerically obtained for the cases of 20cm and 60cm in effective sectional depth. In the case of 20cm, there is no diagonal crack in the analytical result either, whereas, in the case of 60cm, diagonal cracking occurs. In the analysis, when the diagonal crack reached the extreme fiber in compression, the computation ended. Therefore, analysis in the case of an effective sectional depth of 60cm also shows that strength is determined by diagonal crack initiation and propagation; that is to say, shear fracture occurs. With effective sectional depths more than 60cm, the strength is governed by diagonal cracking.

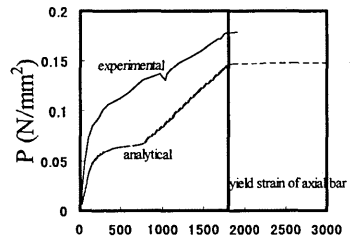

d=20cm

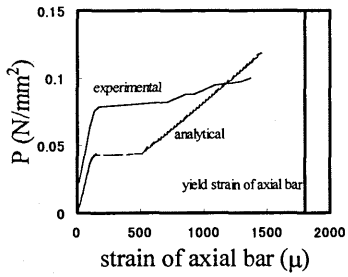

d=60cm

Fig.30 Relationships between Load and Strain of Axial bars

The relationship between principal reinforcement strain and load is shown in Fig.30. In the case of a 20cm effective sectional depth, the analytical results show that the axial reinforcement strain certainly reaches the yield point (1800μ), whereas in the experiment, measurement became impossible when the axial reinforcement strain exceeded the yield point. Thus, both numerically and experimentally, the strength is governed by bending fracture. In the case of a 60cm effective sectional depth, the ultimate strain of the axial reinforcement is below the yield point both numerically and experimentally. Hence, the strength is determined by shear failure. As shown in Fig.30, the strain of the axial reinforcement is generally smaller in the analytical results than in the experimental data. In the real world, cracks around the reinforcement may begin from near indents and develop radially. A three-dimensional model would be necessary to follow such crack propagation. Our study using a two dimensional model cannot correctly evaluate the effect of cracks around reinforcement, and this may be one reason for the disagreement between experimental and analytical results. Another possible reason is that, in the experiment, axial reinforcement is arranged in multiple layers, whereas in the analysis no multiple-layer reinforcement effect was involved. We will study these problems in future by expanding the analytical model into a three-dimensional model.

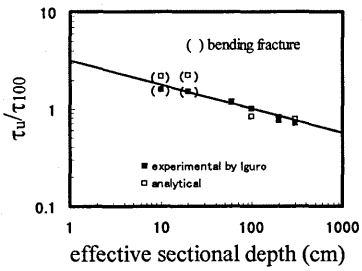

Fig.31 Size Effect of Shear Strength

Figure 31 shows the relationship between concrete shear strength and effective sectional depth. The solid line in the figure represents the size effect of concrete shear strength as proposed by Iguro et al. on the basis of the experimental results. The analytical results agree well with the experimentally determined size effect. This verifies the effectiveness of the proposed model for computing the size effect on the shear strength of RC beams.

4.2 Analysis of Deep Beams

Walraven et al. [16] conducted bending tests for the purpose of investigating the size effect on the shear strength of deep beams. The proposed model was applied to these tests to study the shear strength size effect. Figure 32

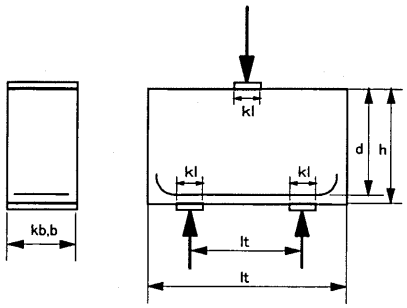

Fig.32 Schematic Diagram of Bending Test of Deep-Beam

Table 7 Test Specimen Dimensions and Physical Properties

h	d	l	b	lt	kl	As	fc
mm	mm	mm	mm	mm	mm	mm^2	N/mm^2
200	160	680	250	320	50	606	18.1
400	360	1030	250	720	100	1020	19.9
600	560	1380	250	1120	150	1570	19.8
800	740	1780	250	1480	200	2040	19.4
1000	930	2250	250	1860	250	2510	20.0

is a schematic diagram of the tests. Table 7 shows the test conditions used in the analysis. Fluctuations in compressive strength are found in the experimental results, and the analysis adopts the average value, 19.4MPa. Since an arch strut is formed in deep beams, the results are influenced by the compressive fracture characteristics of concrete. The present paper does not discuss these compressive fracture characteristics, so its applicability to components dominated by compressive fracture characteristics should be investigated separately. However, according to the analytical results, an arch strut is barely formed in the case discussed here, so it can be estimated that the influence of compressive fracture characteristics of the concrete are in; significant.

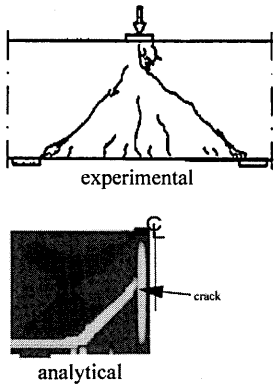

Fig.33 Cracking Status (h=600mm)

Figure 33 is the crack initiation pattern. In the experiments, after bending cracks occured, diagonal cracks were generated. At the end of the experiment, the diagonal cracks and cracks just below the loading plate ran through the specimen, as shown in the figure. In the analysis, after cracks due to bending occur, as in the experiment, a diagonal crack occurs and joins with the bending crack, which grows from the base just below the loading plate toward the upper face. Finally, the computation stops because the diagonal crack attains the loading point, as shown in the figure. Figure 34 is the size effect expressed by the relationship between shear strength and sectional depth. Good agreement is obtained between the analysis and Walraven's experiment for the size effect.

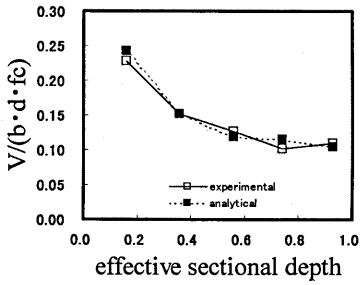

Fig.34 Size Effect of Shear Strength

The above discussions have demonstrated that the proposed analytical model is capable of estimating the cracking pattern in Mode I, Mode II, and mixed, mode situations. In addition, the discussion has verified the applicability of the model to the evaluation of the size effect on the shear strength of RC beams.

5. CONCLUSIONS

In this paper, a smeared crack model is proposed in which cracking may occur at any location, unlike the discrete crack model for which the cracking position must be determined in advance. The proposed model is designed to analyze cracking in Mode I, Mode II, and mixed mode structures where these two modes appear simultaneously. The applicability of the model was verified. Furthermore, by applying the model to RC structures, its effectiveness was demonstrated as regards the analysis of structures with the shear fracture mode, the ultimate strength of which is governed by diagonal crack propagation. The conclusions of this study can be summarized as below.

(1) By considering the transmission of shear force across the crack surface using a smeared crack model, it is possible to analyze diagonal cracking. Instead of a constant shear stiffness, this analysis involves a shear stiffness which decreases with increasing crack opening, like the tension softening curve. The results agree well with experimental results.

(2) By incorporating into the proposed model a reinforcement model based on truss elements that have no bending stiffness, it can be used to determine the fracture behavior of RC structures.

(3) The proposed model was applied to earlier experimental results for RC components. Through a comparison of numerical and experimental results, it is confirmed that the numerical cracking patterns and ultimate strengths are reasonable values.

Acknowledgment

We would like to extend our thanks to the very instructive guidance provided by Professor Horii at the Civil Engineering Section, in the Engineering Department of Tokyo University.

References

[1] Japan Concrete Institute : Report of Committee for Research on Application of Fracture Mechanics, JCI, 1993 (in Japanese)
[2] Uchida, Y., Rokugo, K., and Koyanagi, W., "Study by Fracture Mechanics on the Size Effect of Bending Strength of Concrete", Proceedings of JSCE, No.442/V-16, pp.101-107, 1992 (in Japanese)
[3] Research Committee of Simultaneous Excavation-Lining Method : Design and Operation Method for Simultaneous Excavation-Lining (for urban tunnels), Yoshii-Shoten, 1992 (in Japanese)
[4] Niwa, J., Zareen, N., and Tanabe, T., "Size Effect Analysis of Shear Strength of Concrete Beams Based on Fracture Mechanics", Proceedings of JSCE, No.508/V-26, pp.45-53, 1995 (in Japanese)
[5] An, X., Maekawa, K., and Okamura, H., "Numerical Simulation of Size Effect in Shear Strength of RC Beams", J. Materials, Conc. Struct., Pavements, JSCE, NO.564/V-35, pp.297-316, 1997
[6] Hordijk, P.A., "Local Approach to Fatigue of Concrete", Doctoroal Thesis, Delft University of Technology, 1991
[7] Hori, H., "Problem of Fracture Zone and Systematization of Fracture Mechanics of Concrete, Rock and Ceramics", Proceedings of Structural Engineering, Vol.35A, 1989 (in Japanese)
[8] Planas, J., Guinea, G.V., and Elices, M., "Rupture Modulus and Fracture Properties of Concrete", Fracture Mechanics of Concrete Structures, Proceedings FRAMCOS-2, edited by Folker H. Wittmann, AEDIFICATIO publishers, pp.95-110, 1995
[9] Watanabe, T., Matsuoka, S., and Takeda, Y., "Study on Shear Strength of Reinforced Concrete Based on Fracture Mechanics", Proceedings of JSCE, No.592/V-39, pp.25-36, 1998 (in Japanese)
[10] Arrea, M, and A. R. Ingraffea, "Mixed-mode crack propagation in mortar and concrete", Report No.81-13, Department of Structural Engineering, Cornell University, Ithaca, New York, 1982
[11] Koenig, G., Grimn, R., and Remmel, G., "Shear Behavior of Longitudinally Reinforced Concrete Members of HSC", JCI International Workshop on Size Effect in Concrete Structures, pp.63-74, 1993
[12] Helbing, A., Alvaredo, A.M., and Wittmann, F.H., "Round Robin Test of Anchor Bolts, Round-Robin Analysis of Anchor Bolts", RILEM TC-90 FMA Fracture Mechanics of Concrete-Applications, Preliminary Report, 1991
[13] Wittmann, F.H., Roelfstra, P.E., Mihashi, H., Huang, Y-Y., Zhang, X-H., and Nomura, N., "Influence of Age of Loading, Water-Cement Ratio and Rate of Loading on Fracture Energy of Concrete, Materials and Structures, vol.20, No.116, pp.103-110, 1987
[14] Shima, H., Chou, L., and Okamura, H., "Micro and Macro Models for Bond in Reinforced Concrete", Journal of The Faculty of Engineering, The University of Tokyo (B), Vol.XXXIX, No.2, pp.133-194, 1987
[15] Iguro, M, Shioya, T., Nojiri, Y., and Akiyama, H., "Experimental Study on Large Reinforced Concrete Beams under Uniform Load", Proceedings of JSCE, No.348/V-1(Report), pp.175-184, 1984 (in Japanese)
[16] Walraven, J.C., "Size Effects : Their Nature and Their Recognition in Building Codes", Size Effect in Concrete Structures, Edited by H.Mihashi, H.Okamura, and Z.P.Bazant, pp.375-394, 1994